Received: 1 December 2023 | Revised: 6 March 2024 | Accepted: 22 March 2024

Micro & Nano Letters

DOI: 10.1049/mna2.12197

The Institution of Engineering and Technology WILEY

LETTER

Upcycling prawn shells: Chitosan–carbon nanotube nanocomposites with boosted magnetic and electrical properties

Rabiul Awal[1,2] | Md. Al-Mamun[3] | Nasrin Jewena[4] | Jahirul Islam Khandaker[2] | Nilufer Yesmin Tanisa[1,2] | Shamim Ahmed[1] | Fahim Shahriar[5] | Md. Mahbubul Haque[3]

[1]Department of Physics, Uttara University, Dhaka, Bangladesh

[2]Department of Physics, Jahangirnagar University, Dhaka, Bangladesh

[3]Materials Science Division, Atomic Energy Centre, Dhaka, Bangladesh

[4]Department of Chemistry, Jahangirnagar University, Dhaka, Bangladesh

[5]Department of Nuclear Engineering, Military Institute of Science and Technology, Dhaka, Bangladesh

Correspondence
Rabiul Awal, Department of Physics, Uttara University, Dhaka 1230, Bangladesh.
Email: rabiulnanophy@gmail.com

Abstract

Multi-walled carbon nanotubes (MWCNTs) were successfully synthesized and functionalized by chemical vapour deposition and acid reflux methods, respectively. Chitosan (CTS) was prepared by a chemical extraction method from waste prawn shells. Various weight fractions of functionalized multi-walled carbon nanotubes (f-MWCNTs) have been used as reinforcing agent in CTS biopolymer matrix. Fourier transform infrared spectroscopy analysis was done, which confirms the presence of absorption bands of the various functional groups of chitin, CTS, and MWCNTs. Raman spectra revealed the quality of MWCNTs, the extent of their functionalization, and the quality of nanocomposites. The X-ray diffraction analysis showed the distinctive peaks for f-MWCNTs' and also revealed the formation of CTS/f-MWCNTs nanocomposites. Transmission Electron Microscopy (TEM) analysis also exhibited that the CTS/f-MWCNTs nanoparticles have a well-defined crystalline structure. The highest coercivity and magnetization (Ms) of the CTS/5%f-MWCNTs nanocomposite are 602 Oe and 0.1202 emu/g, respectively that have been enhanced by 3.83 and 5.27 times compared to the pure CTS respectively. It showed that the conductivity is getting higher with the addition of f-MWCNTs in the CTS matrix. CTS/5% f-MWCNTs composites exhibit the highest conductivity than other composites and the conductivity of CTS/5% f-MWCNTs composite is 4.0×10^{-4} S/m.

1 | INTRODUCTION

Synthetic polymer-based composites are created by incorporating various fillers to enhance specific properties for lithium-ion batteries [1, 2]. Recent research works are increasingly concentrating on the advancement and application of biopolymers derived from natural sources [3, 4]. Biopolymers have attracted considerable interest due to its multifaceted attributes such as biocompatibility, biodegradability, and low toxicity [5]. Scientists have already synthesized some composites reinforced with inorganic fillers aimed at the development of specific properties for various purposes. Researchers studied the effect of magnetite nanoparticles on the electrical, magnetic, and thermal characteristics of chitin/cashew gum biopolymer nanocomposites [6].

Among the many available bio-based polymers, Chitosan (CTS) bio-polymer exhibits exceptional properties. Chitin and CTS have also been used as absorption substances to eliminate organic dyes from industrial wastewater [7]. To remove ferrous (Fe II) and manganese (Mn II) metal ions from water, CTS nanoparticles are considered to be an effective, economical, safe, and environmentally suitable product [8]. Several researchers in their review article investigate the latest advancements in the creation of polymeric nanocomposites based on CTS and assess their effectiveness in eliminating a wide range of pollutants, such as heavy metals, dyes, pesticides, pharmaceutical residues, and radioactive substances, from water sources [9–11].

CTS, a naturally derived biopolymer with inherent biocompatibility and biodegradability, has garnered significant interest in various advanced material applications [12]. However, its inherent limitations, such as poor magnetic susceptibility and low electrical conductivity, frequently prevent it from reaching its full potential. Carbon nanotubes (CNTs) and CTS together

offer an intriguing way to get beyond these restrictions and create multifunctional composites with customized magnetic and electrical properties. CTS-based nanocomposites are one of the most valuable nanocomposites in the present world due to their non-toxic, biocompatible, biodegradable, physical, and mechanical properties [13–15]. CNTs, known for their exceptional electrical conductivity, high aspect ratio, low density, high stiffness, and diverse magnetic functionalities, can act as synergistic reinforcements within the CTS matrix [16, 17]. This synergistic blend creates opportunities for a wide range of potential applications, including electromagnetic interference (EMI) shielding, bioelectronics, and magnetic materials [18].

CTS and pure CNT-based nanocomposites have demonstrated essential mechanical and electrical characteristics [19, 20]. According to published research, CTS can aid to prevent f-MWCNT clumping by allowing for the uniform distribution of functionalized multi-walled carbon nanotubes (f-MWCNTs) inside the matrix [21]. The electrical conductivity of these composites has increased when CTS is added together with f-MWCNTs. This characteristic is essential for applications such as electromagnetic shielding, flexible electronics, and conductive polymers. Due to their superior thermal conductivity, f-MWCNTs can enhance heat dissipation in materials [22]. Their electrical conductivity and biocompatibility render them appropriate for a multitude of sensor applications, encompassing healthcare and environmental monitoring. Because CTS-MWCNT composites are robust and lightweight, they are useful in applications where reducing weight without sacrificing structural integrity is essential [23, 24]. The automotive, sporting goods, and aerospace industries can benefit from this. There are a lot of opportunities in many industries when CTS and f-MWCNTs are combined [21]. Good strength, light weight, and occasionally electrical conductivity are necessary for the composite to be used in biological applications so that it can self-heal. f-MWCNTs have excellent properties that can be utilized to make these composites.

A significant advance in the field of cutting-edge scientific study has given rise to the intriguing domain of prawn-derived CTS biopolymer-based nanocomposites. These unique materials, which are loaded with aligned domains of f-MWCNTs, are carefully prepared using an advanced chemical technique. This innovation promises to reshape the landscape of materials science, as the ratios of CTS to f-MWCNTs employed in the fabrication of these nanocomposites wield a profound influence over their magnetic and electrical properties. This combination combines the exceptional electrical and magnetic characteristics of carbon nanotubes with the biopolymer CTS. The final product has improved magnetic sensitivity and electrical conductivity.

2 | MATERIALS AND METHOD

2.1 | Materials

In this study, sodium hydroxide 99.97% (CAS-1310-73-2/106462) hydrochloric acid (HCl) having strength of 37 % (CAS-100317) and acetic acid (glacial) 100% (CAS- 64-19-7/137000), all from Merck KGaA, Germany, were used. They were diluted with distilled water to the concentration necessary for the different procedures. On quartz substrates, MWCNTs were created using the chemical vapour deposition (CVD) technique at 760°C [25]. In order to functionalize the MWCNT, sulfuric acid (H_2SO_4) and nitric acid (HNO_3) of analytical grade were purchased from Merck, Germany.

2.2 | Sample preparation

Functionalization of MWCNTs: Previous investigations [26, 28] demonstrated that MWCNTs were acid-functionalized in a variety of circumstances, including high reflux temperatures of 80 to 150°C for 8 to 48 h. MWCNTs were functionalized in this work using the following steps sonication with the acid mixture and acid reflux of the dispersed solution.

Sonication with H_2SO_4 and HNO_3: In an Erlenmeyer flask, concentrated H_2SO_4 and HNO_3 were combined at a 3:1 (V/V) ratio, along with 500 mg of MWCNT. This combination was then sonicated for 4 h at a standard temperature in an ultrasonication bath. After being sonicated, the mixture was left alone for a full 12 h.

Acid reflux procedure: After that, the evenly distributed mixture was poured into a flask with three necks, a thermometer, a round bottom, and a reflux condenser. Utilizing a heating mantle, 8 h was spent refluxing the mixture at 80°C. The distributed solution was cooled after that, and a centrifuge was used to separate the nanotubes from the acidic solution. The nanotubes were dried for 12 h at 100°C after being rinsed in deionized water until the pH was neutral. The dehydrated f-MWCNTs were characterized and prepared for applications in the fabrication of nanocomposites. The product was then baked for 24 h at 105°C. Chitin was produced from prawn shell powder by the process of deproteination and demineralization methods [29, 30]. The prepared chitin is a phased product used to make CTS. The chitin was deacetylated using 1 N NaOH (chitin: NaOH = 1:20, w/v) at 100°C for 4 h to produce CTS. The resulting solid CTS was then dried in a vacuum oven for 24 h at 50°C. The as-prepared CTS powders were analyzed using Fourier transform infrared spectroscopy (FT-IR) (Section 2.3) for confirmation of their preparation (compared with standard FT-IR scans of CTS) [31, 32]. The pristine multi-walled carbon nanotubes (p-MWCNTs) were functionalized by HNO_3 using a method established by Zaman et al. and Montoro and Rosolen [33, 34]. The p-MWCNTs, with an average size of 1 nm and 1.2 μm, were sonicated in a beaker filled with concentrated HNO3 (65%, 30 mL) for 30 min. The carboxyl functional groups (MWCNT-COOH) were then added to the dispersed solution by heating it to 90°C and refluxing it for 4 h. The resulting p-MWCNTs-COOH was washed until the pH = 6.0, followed by 2n acetone wash, and then dried at 65°C for 24 h. The nanocomposites of f-MWCNTs and CTS, with compositions CTS/1%f-MWCNTs, CTS/3%f-MWCNTs, and CTS/5%f-MWCNTs, were produced using a modified version

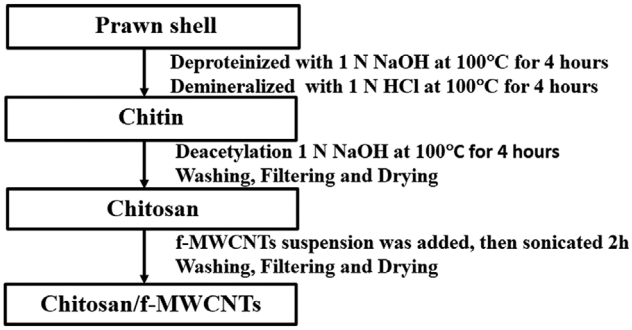

FIGURE 1 Flowchart for the sample preparation process.

of the method described by Wang et al. [35]. The f-MWCNTs were homogenized in an ultrasonic bath for 60 min after being initially swollen in 100 mL of distilled water. This f-MWCNT suspension was then mixed with 1 g of CTS and 1 mL of an acetic acid solution, followed by sonication for 20 min to eliminate bubbles. The CTS/f-MWCNTs solutions were then filtered in a vacuum membrane filter unit utilizing a 0.2-μm membrane (nylon 6:6). The resultant filtrate was next heated at 60°C for 24 h, dried, and processed by hand for roughly an hour to produce powders. Figure 1 depicts the flowchart for the sample preparation process.

2.3 | Characterization techniques

The MWCNTs, f-MWCNTs, and as-prepared nanocomposite powders were studied directly by an ATR (attenuated total reflection) method using an IR Ptrestige-21 FT-IR (Bara Scientific Co., Ltd., Japan) for the confirmation of the chemical and structural nature of the samples with scanning over a spectral range of 4000 to 350 cm^{-1} at a best resolution of 0.5 cm^{-1} per 5 s.

X-ray diffraction (XRD) (X'pert PRO x-ray diffractometer (PW3040), Philips Pan Analytical Co., Ltd.) was used to analyze the physical structure and phase of the powder samples (The Netherlands), using Cu K_{α} source of x-ray wavelength of 0.15406 nm and all samples were continuously scanned (1D mode) at a rate of 2°/min with a width of 0.02°over a 2θ range of 5° to 90°.

To examine the vibrational frequency of a bond in a molecule, the samples underwent characterization through Raman spectroscopy using the MonoVista CRS + confocal Raman microscope within the suitable range.

Transmission Electron Microscopy (TEM) (TALOS F200 G2, Thermo Fisher Scientific, USA) technique was used to study the internal structure of a wide range of materials at the nanoscale. By using vibrting-sample magnetometer (VMS) (EV-9, Microsense Co., Ltd. USA) analysis, magnetic properties including magnetization, coercive force, and hysteresis loop were investigated. Using an impedance analyzer (6500B series, Wayne Kerr Electronics Co., Ltd., UK), electrical characteristics including frequency-dependent conductivity and resistivity of all samples were examined.

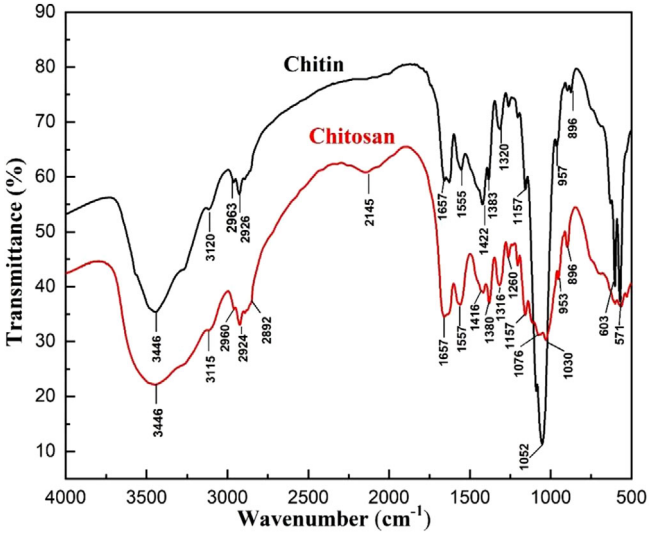

FIGURE 2 FT-IR spectrum of chitin and chitosan. FT-IR, Fourier transform infrared spectroscopy.

3 | RESULT AND DISCUSSION

3.1 | FTIR analysis

3.1.1 | FTIR absorption studies of chitin and CTS

Many researchers have investigated the absorption bands of the functional groups in chitin and CTS and compared them with their standard absorption bands [32]. Figure 2 shows the FT-IR spectra of chitin and CTS.

The chitin spectrum proved its successive extraction from the shrimp shells. The investigation confirmed the chitin characteristic absorption bands at 1551 (amide II), 1674 cm^{-1} (C═O) stretch, and C═O and NH stretching vibrations in the NHCOCH side groups were observed at 3085 and 3265 cm^{-1}, respectively. The stretching vibrations of C—H at 2916 cm^{-1} and its bending vibrations at 1415 and 1375 cm^{-1} in CTS were found by Teli and Sheikh [31]. According to Al-Sagheer et al. [36] the major absorption bands of CTS are at 3444, 2919, 1659, 1420, 1080, and 1033 cm^{-1}. In Figure 2, the major absorption bands of our CTS were observed at 3446,2924, 1657, 1416, 1076, and 1030 cm^{-1} all nearly identical to theirs. From the comparison of our FT-IR spectra with other researchers, it was found that most of the absorption bands of our synthesized CTS are similar.

3.1.2 | FT-IR study of p-MWCNTs and f-MWCNTs

FT-IR spectroscopy was used to determine the p-MWCNTs and f-MWCNTs' chemical and structural properties (Figure 3). A large peak at 3464 cm^{-1} was observed for the O-H stretching of the hydroxyl group from carboxyl groups (O═C—OH and C—OH). The

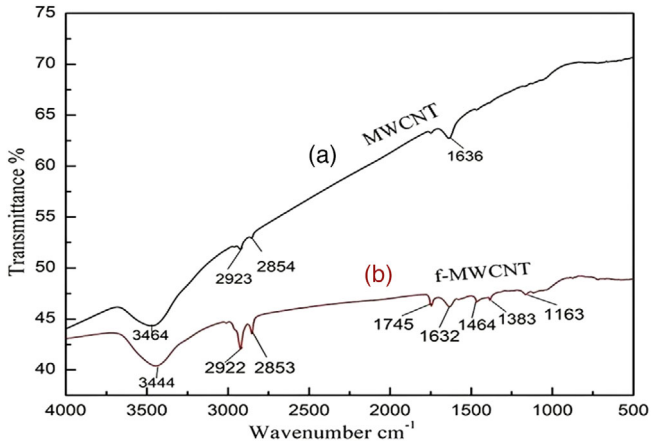

FIGURE 3 FT-IR spectra of MWCNT (curve a) and f-MWCNT (curve b). f-MWCNTs, functionalized multi-walled carbon nanotubes; FT-IR, Fourier transform infrared spectroscopy; MWCNT, multi-walled carbon nanotubes.

partial oxidation that occurred during the purification p-MWCNTs left them with carboxyl groups on their surface [37]. The occurrence of the C═O and C—O stretching modes of vibration was explained by the presence of two extra peaks at 1745 and 1163 cm^{-1} in the f-MWCNTs spectra shown in Figure 3 (curve b) [38]. The absorption peak at 1636 cm^{-1} was attributed to the stretching of the —CH_2— group in the hexagonal lattice of the carbon nanotube backbone, and the peak at 2922 cm^{-1}, which denoted the presence of a long-chain alkyl molecule, to the C—H stretch modes of the H—C═O in the carbonyl group [37].

3.1.3 | FT-IR study of CTS/f-MWCNTs composites

The FT-IR spectra of CTS and f-MWCNTs were subjected to individual analysis, revealing distinct vibration bands. In the case of CTS, the characteristic vibration bands were identified at 3446, 3115, 2960, 2924, 2892, 2145, 1657, 1557, 1416, 1380, 1316, 1076, and 1030 cm^{-1} (as shown in Figure 2, curve a). Conversely, for all f-MWCNTs, the vibration bands appeared at 3444, 2922, 2853, 1745, 1632, 1464, 1383, and 1163 cm^{-1} (as depicted in Figure 3, curve b). Absorption bands of 3450, 3267, 3112, 2962, 2928, 2892, 1657, 1626, 1557, 1416, 1380, 1315, 1073, and 1027 cm^{-1} were observed in the prepared CTS/f-MWCNTs composites (Figure 4) which are close to the absorption bands determined by Thou et al. and Osler et al. [39, 40].

3.2 | Raman analysis

The spectral response of MWCNT and f-MWCNT is shown in Figure 6, with the three common characteristic bands D-band, G-band, and G′ band displayed. The D-band is shown at 1355 cm^{-1} in Figure 5a, which is seen in the results from an augmented vibrational mode connected to graphene edges and suggests that the graphene structure is somewhat disordered. The breathing mode of the sp^3 sites that are present in rings in carbon tubes is associated with this band, which is also known as the disorder band [40]. The G-band, which is observed to be at 1581 cm^{-1} in Figure 5a and results from the sp2 bonds in graphene sheets being stretched in-plane tangentially, indicates the distinctive graphitic structure of carbon allotropes [41]. The two TO phonons involved in the double resonance-enhanced two-phonon process close to the K point are what causes the noticeable G′-band at 2666 and 2681 cm^{-1} in Figures 5a and 5b, respectively. As demonstrated in Figure 5b, the f-MWCNT's Raman spectra exhibit bands at 1356 (D-band) and 1582 cm^{-1} (G-band). The D-band to G-band intensity ratio (ID/IG) serves as a proxy for the disorder and defect density present in nanotube structures. Functionalization has caused the ID/IG ratio to increase from 0.82 to 0.88. After functionalization, the defect density increased, and the fact that this ratio did to indicate that the tubes were properly functionalized by adding various functional groups.

3.3 | X-ray diffraction analysis

Figure 6 displays the XRD patterns of pure CTS, f-MWCNTs, and CTS/f-MWCNT composites. The diffraction pattern of pure CTS shows peaks at 2θ = 20°, 24°, 26°, and 39° indicating the ordered crystalline structure of CTS [42]. The f-MWCNTs have the characteristic peaks of carbon at 26° and 42° (PAN-ICSD Ref. code 98- 008–5678). Because the sample's carbon atoms have (002) planes arranged in a tubular form, the peak at 26° is the typical graphitic peak. The (101) planes of the nanotube structure are thought to be responsible for the peak at about 42° [43]. The CTS/f-MWCNTs composite has good crystallinity, as seen by the main peak 2θ = 20° for the CST/f-MWCNTs pattern, which is a characteristic peak of raw-CTS and is still intense and crisp. In composites, the reduction of the intensities of corresponding peaks of CTS and f-MWCNTs indicates the formation of CTS/f-MWCNTs composites [44]. The more the loading of f-MWCNTS increases in the composites the characteristic peaks (2θ = 26° and 42°) of carbon nanotubes are more evident in Figure 6.

3.4 | TEM analysis

Figure 7 presents TEM, high-resolution TEM (HRTEM) images, and selected area electron diffraction (SAED) patterns of CTS and the CTS/f-MWCNTs composite. In Figures 7a and 7d show the TEM images of CTS and CTS/f-MWCNTs. In Figure 7b, the HRTEM image of CTS indicates a d-spacing of approximately 4.50 Å, corresponding to the (110) plane. For f-MWCNTs, shown in Figure 7e, the d-spacing measures 3.51 Å, corresponding to the (002) plane [44]. The HRTEM image of the CTS/f-MWCNTs composite in Figure 7e shows d-spacings of 4.50 and 3.51 Å, corresponding to the crystal planes (110) and (002), respectively. This is further validated by the SAED pattern of the CTS/f-MWCNTs composite in

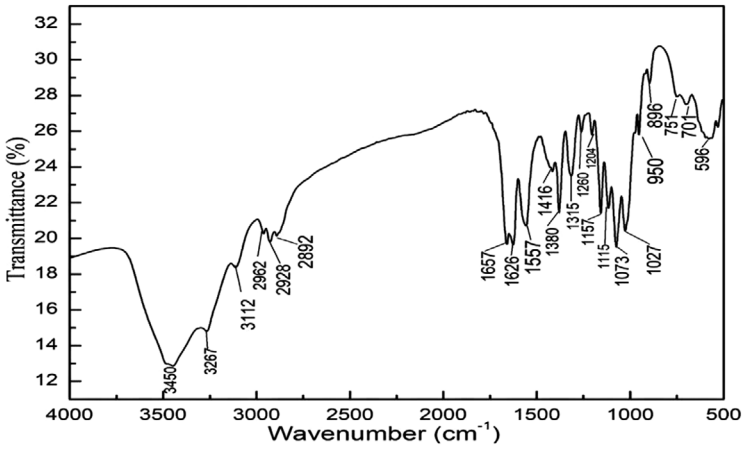

FIGURE 4 FT-IR spectrum of chitosan/f-MWCNT composites. f-MWCNTs, functionalized multi-walled carbon nanotubes; FT-IR, Fourier transform infrared spectroscopy.

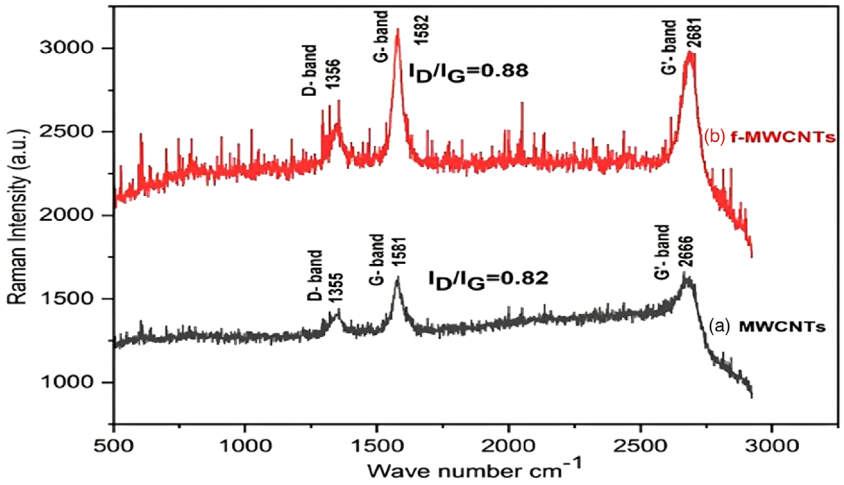

FIGURE 5 Raman spectra of a. MWCNTs and b. f-MWCNTs. f-MWCNTs, functionalized multi-walled carbon nanotubes; MWCNTs, pristine multi-walled carbon nanotubes.

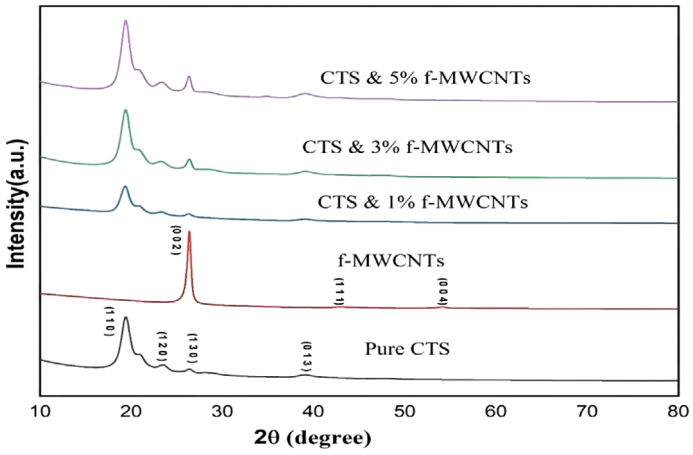

FIGURE 6 Displays the XRD patterns of pure CTS, f-MWCNTs, and CTS/f-MWCNT composites. CTS, chitosan; f-MWCNTs, functionalized multi-walled carbon nanotubes; XRD, X-ray diffraction.

Figure 7f. In the SAED pattern of the CTS composite, concentric circles are observed, indexed as (110), (120), (002), (130), and (004) lattice planes. These circles correspond well with the XRD data. Therefore, the SAED pattern indicates that the CTS/f-MWCNTs nanoparticles possess a fully crystalline structure. An agglomeration of nanoparticles within the polymer occurs as a result of the blend matrix's developing stress due to particle-to-particle interactions [6].

3.5 | Analysis of magnetic properties: vibrating sample magnetometer analysis

Figures 8 and 9 depict the relationship between magnetization (M) and applied magnetic field (H) for f-MWCNTs, CTS, and the composites CTS/1% f-MWCNTs, CTS/3% f-MWCNTs, and CTS/5% f-MWCNTs. In Figure 8, the hysteresis curve of f-MWCNT reveals a paramagnetic nature, showcasing a

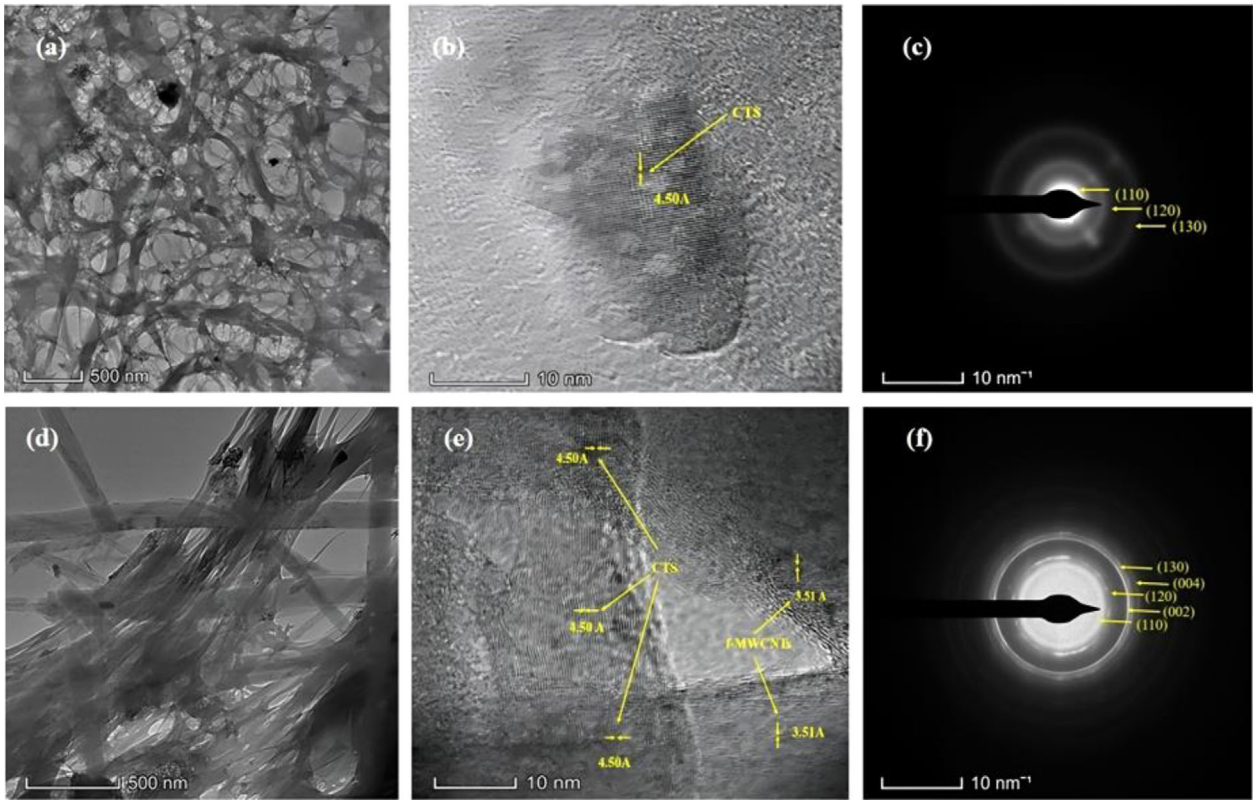

FIGURE 7 TEM images of (a) chitosan, (d) chitosan/f-MWCNTs composite; HRTEM images of (b) chitosan, (e) chitosan/f-MWCNTs composite; SAED pattern of (c) chitosan, (f) chitosan/f-MWCNTs composite. f-MWCNTs, functionalized multi-walled carbon nanotubes; HRTEM, high-resolution transmission electron microscopy; SAED, selected area electron diffraction; TEM, transmission electron microscopy.

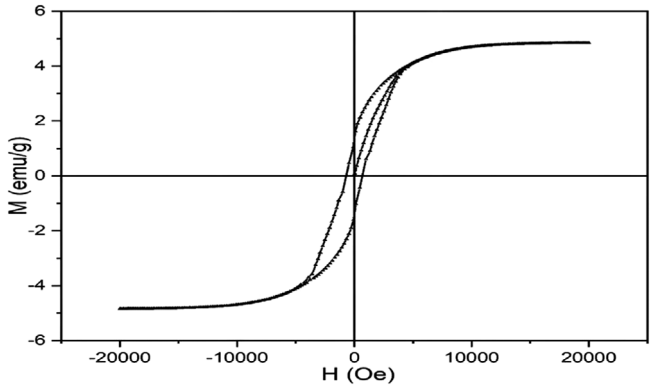

FIGURE 8 Magnetic hysteresis loop of f-MWCNTs. f-MWCNTs, functionalized multi-walled carbon nanotubes.

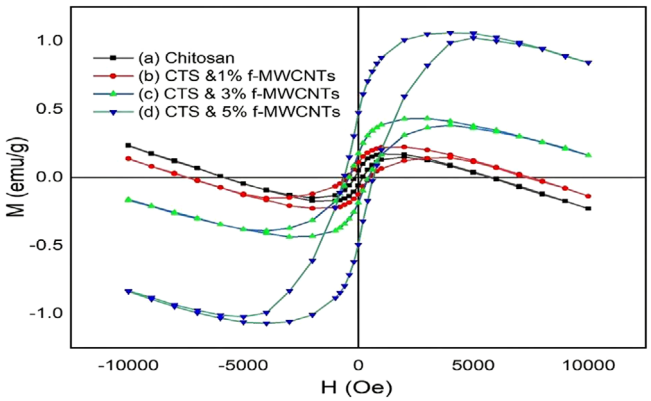

FIGURE 9 Comparison of hysteresis curves of pure chitosan and CTS/1% f-MWCNTs (a), CTS/3% f-MWCNTs (b), and CTS/5% f-MWCNTs (c) composites. CTS, chitosan; f-MWCNTs, functionalized multi-walled carbon nanotubes.

saturation magnetization of the nanotube [45, 46]. When 1% of f-MWCNTs were added to the CTS, this composite's hysteresis curve was very different from the pure CTS's (Figure 8). This sample exhibited twice as much magnetization as CTS and it was also observed that the shape of the magnetization curve was changed by the applied field up to 10KOe at room temperature. As also shown in Figure 9, with a rise in f-MWCNT content, the compositions' magnetic characteristics, saturation magnetization, and coercivity increased. All three compositions had large hysteresis loops after adding f-MWCNTs. The magnetic hysteresis curves were used to determine the coercivity (Hc (Oe), saturation magnetization (Ms (emu/g), and remanence (Mr (emu/g), which are all shown in Table 1. This phenomenon can be ascribed to the correlation between Ms, which represents the saturation magnetization of an individual particle, and the volume fraction, denoted as Ms = Φ ms [47].

It was observed that Hc of CTS was 157 Oe, for f-MWCNTs Hc = 690 Oe, CTS/1%f-MWCNTs was

TABLE 1 Magnetic properties obtained from VSM measurements.

Sample name	Coercivity Hc (Oe)	Magnetization Ms (emu/g)	Remanence Mr (emu/g)
Chitosan (CTS)	157	0.0228	0.0055
f-MWCNTs	690	4.96	1.45
CTS and 1% f-MWCNTs	391	0.0289	0.0117
CTS and 3% f-MWCNTs	438	0.0524	0.0181
CTS and 5% f-MWCNTs	602	0.1202	0.0484

Abbreviations: CTS, chitosan; f-MWCNTs, functionalized multi-walled carbon nanotubes.

Hc = 391 Oe, for 3%f-MWCNts Hc = 438 Oe, and for 5% f-MWCNTs Hc = 602 Oe. These magnetic measurements clearly show that the magnetic parameters were affected by the reinforcing of f-MWCNTs onto the low magnetic CTS matrix [48]. Coercivity irregularities can be related to numerous reasons, including magneto crystalline anisotropy, CTS- f-MWCNTs content ratio, distinct types of domain development, and particle size [45]. The Hc increased with the increase of f-MWCNTs. Such a composite material with high Hc and Ms would be ideal for electromagnetic waves absorption application and water filtration of magnetic contaminants such as iron, cobalt, nickel, and their oxides.

3.6 | Analysis of electrical properties

The resistivity of CTS biopolymer is very high being equivalent to 10^5 ohm-m. Hu et al. [49] showed that the resistivity of chitosan-reinforced Ti3C2X films was increased gradually with the increase of CTS. Even dispersing small amounts of CNTs into insulating polymers can effectively reduce the electrical resistivity of polymeric matrices [50]. The frequency-dependent resistivity (ρ) was measured at room temperature for the CTS/1%f-MWCNTs, CTS/3%f-MWCNTs, and CTS/5%f-MWCNTs composites sintered at 150°C for 1 h in an oven in the form of sheets about 0.5 to 1.0 mm thick. The variation of resistivity through the sheets with the applied frequency is shown in Figure 10. In this study, the resistivity of the CTS/1%f-MWCNTs sample at low frequencies was very high, and as soon as the frequency increased, the resistivity began to decrease. Up to a frequency of 600 kHz, the resistivity decreased at a high rate. On the other hand, the decay of the resistivities of the samples doped with 3% and 5% f-MWCNTs was very small with the increase of frequency (Figure 10). The resistivities of CTS/1%f-MWCNTs, CTS/3%f-MWCNTs, and CTS/5%f-MWCNTs composites at a frequency of 9.0×10^5 Hz are 7.5×10^3, 3.0×10^3, and 2.5×10^3 ohm-m, respectively as shown in Figure 10. The saturation of resistivity was exhibited at the higher percentage of f-MWCNTs within the composites. Thus, they were very different from the CTS/1%f-MWCNTs for which the resistivity decreased sharply with the increase in frequency. The reciprocal of resistivity gives the conductivity. The conductivities of CTS/1%f-MWCNTs, CTS/3%f-MWCNTs, and CTS/5%f-MWCNTs composites at a frequency of 9.0×10^5 Hz are 1.33×10^{-4}, 3.33×10^{-4}, and 4.0×10^{-4} S/m, respectively, and these values were compared to the other studies [51, 52].

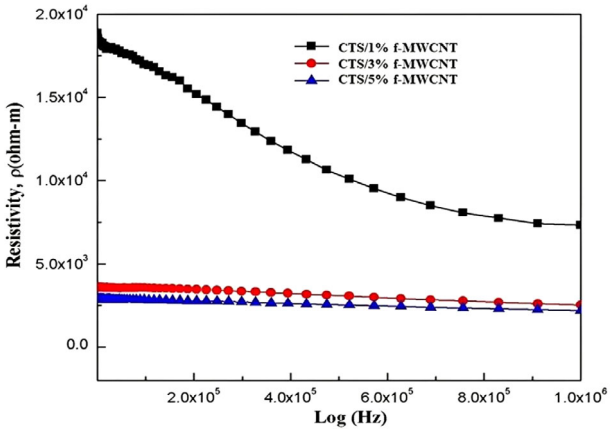

FIGURE 10 Variation of resistivity (ρ) with frequency (log f) for CTS/1%f-MWCNTs, CTS/3%f-MWCNTs, and CTS/5%f-MWCNTs composites. CTS, chitosan; MWCNTs, multi-walled carbon nanotubes.

4 | CONCLUSIONS

CTS is one of the useful biopolymers that have most of the valuable properties of polysaccharides such as non-toxicity, biocompatibility, and biodegradability. In the ongoing study, CTS was purified as a white powder from prawn shells. After adding f-MWCNTs in three different ratios (1, 3, and 5)% to the CTS, the properties of CTS powder incorporated with f-MWCNT were explored. A modest amount (5%) of f-MWCNTs was added to the CTS composites, specifically altering their magnetic and electrical properties. To thoroughly analyze these composites, detailed examinations were conducted on CTS/1%f-MWCNTs using FT-IR and XRD, while VSM and impedance analysis were employed for CTS/1%f-MWCNTs, CTS/3%f-MWCNTs, and CTS/5%f-MWCNTs. It was determined from the FT-IR investigation that our chitin's absorption bands, which were extracted from prawn shells, were similar to those of standard chitin and it was also confirmed that the CTS vibration bands resembled those of the standard CTS. The MWCNTs treated with nitric acid for 6 h had carboxyl functional groups produced, according to the FT-IR study. HRTEM images reveal specific d-spacing values for CTS and f-MWCNTs, and the composite, indicating their crystal planes. The SAED pattern for the CTS/f-MWCNTs composite confirms a fully crystalline structure with concentric circles corresponding to specific lattice planes, consistent with XRD data. The VSM data showed a saturation point in the magnetic field at less than 10,000 Oe; Ms was 0.1202 emu/g and the Hc was 602 Oe for the CTS/5% f-MWCNTs sample, much higher than that for the other samples. Thus, the magnetic properties of this composite were higher than those of the other samples. For the CTS/1%f-MWCNTs, CTS/3%f-MWCNTs, and CTS/5%f-MWCNTs composites, the conductivities are

1.33×10^{-4}, 3.33×10^{-4}, and 4.0×10^{-4} S/m at a frequency of 9.0×10^{5} Hz, respectively. Finally, the incorporation of f-MWCNTs into CTS resulted in composite materials with altered magnetic and electrical properties, with notable enhancements observed at specific compositions, providing insights for potential applications in various fields.

AUTHOR CONTRIBUTIONS

Rabiul Awal: Methodology; investigation; visualization; writing—original draft. **Md. Al-Mamun**: Conceptualization; methodology; writing—reviewing and editing; supervision; project administration. **Nasrin Jewena**: Writing—review & editing; **Jahirul Islam Khandaker**: Writing—review & editing and supervision. **Nilufer Yesmin Tanisa**: Writing—review & editing. **Shamim Ahmed**: Writing—review & editing. **Fahim Shahriar**: Writing—review & Editing. **Md. Mahbubul Haque**: Writing—review & editing and supervision.

ACKNOWLEDGEMENTS

I would like to thank The International Science Programme (ISP) at Uppsala University, Sweden, and the NST Fellowship, Ministry of Science and Technology, Bangladesh.

CONFLICT OF INTEREST STATEMENT

The authors declare no conflict of interest.

DATA AVAILABILITY STATEMENT

Data sharing not applicable to this article as no datasets were generated or analyzed during the current study.

REFERENCES

1. Masoud, E.M.: Montmorillonite incorporated polymethylmethacrylate matrix containing lithium trifluoromethanesulphonate (LTF) salt: Thermally stable polymer nanocomposite electrolyte for lithium-ion batteries application. Ionics. 25, 2645–2656 (2019). https://doi.org/10.1007/s11581-018-2802-1
2. Masoud, E.M., El-Bellihi, A.A., Bayoumy, W.A., Mohamed, E.A.: Polymer composite containing nano magnesium oxide filler and lithiumtriflate salt: An efficient polymer electrolyte for lithium ion batteries application. J. Mol. Liq. 260, 237–244 (2018,). https://doi.org/10.1016/j.molliq.2018.03.084
3. Amruth, K., Abhirami, K.M., Sankar, S., Ramesan, M.T.: Synthesis, characterization, dielectric properties and gas sensing application of polythiophene/chitosan nanocomposites. Inorg. Chem. Communications. 136, 109184 (2022). https://doi.org/10.1016/j.inoche.2021.109184
4. Hisham, F., Akmal, M.M., Ahmad, F., Ahmad, K., Samat, N.: Biopolymer chitosan: Potential sources, extraction methods, and emerging applications. Ain Shams Eng. J. 15, 102424 (2023). https://doi.org/10.1016/j.asej.2023.102424
5. Budiarso, I.J., Rini, N.D., Tsalsabila, A., Birowosuto, M.D., Wibowo, A.: Chitosan-based smart biomaterials for biomedical applications: Progress and perspectives. ACS Biomater. Sci. Eng. 9, 3084–3115 (2023). https://doi.org/10.1021/acsbiomaterials.3c00216
6. Ramesan, M.T., Privya, P.P., Jayakrishnan, P., Kalaprasad, G., Bahuleyan, B.K., Al-Maghrabi, M.A.: Influence of magnetite nanoparticles on electrical, magnetic and thermal properties of chitin/cashew gum biopolymer nanocomposites. Polym. Compos. 39, E540–E549 (2018). https://doi.org/10.1002/pc.24688
7. Dassanayake, R.S., Acharya, S., Abidi, N.: Biopolymer-based materials from polysaccharides: Properties, processing, characterization and sorption applications. Advanced Sorption Process Applications, 1–24. https://doi.org/10.5772/intechopen.80898
8. Ali, M.E.A., Aboelfadl, M.M.S., Selim, A.M., Khalil, H.F., Elkady, G.M.: Chitosan nanoparticles extracted from shrimp shells, application for removal of Fe (II) and Mn (II) from aqueous phases. Sep. Sci. Technol. 53(18), 2870–2881 (2018). https://doi.org/10.1080/01496395.2018.1489845
9. Mallik, A.K., Kabir, S.F., Rahman, F.B.A., Sakib, M.N., Efty, S.S., Rahman, M.M.: Cu (II) removal from wastewater using chitosan-based adsorbents: A review. J. Environ. Chem. Eng. 10(4), 108048 (2022). https://doi.org/10.1016/j.jece.2022.108048
10. Aramesh, N., Bagheri, A.R., Bilal, M.: Chitosan-based hybrid materials for adsorptive removal of dyes and underlying interaction mechanisms. Int. J. Biol. Macromol. 183, 399–422 (2021). https://doi.org/10.1016/j.ijbiomac.2021.04.158
11. Yaqoob, A.A., Ahmad, A., Ibrahim, M.N.M., Rashid, M.: Chitosan-based nanocomposites for gene delivery: Application and future perspectives. In: Polysaccharide-Based Nanocomposites for Gene Delivery and Tissue Engineering. Woodhead Publishing, pp. 245–262 (2021). https://doi.org/10.1016/B978-0-12-821230-1.00001-3
12. Chadha, U., Bhardwaj, P., Selvaraj, S.K., Kumari, K., Isaac, T.S., Panjwani, M., Kulkarni, K., Mathew, R.M., Satheesh, A.M., Paramasivam, V.: Retracted: Advances in chitosan biopolymer composite materials: From bioengineering, wastewater treatment to agricultural applications. Mater. Res. Express. 9(5), 052002 (2022). https://doi.org/10.1088/2053-1591/ac5a9d
13. Ramachandran, S., Rajinipriya, M., Soulestin, J., Nagalakshmaiah, M.: Recent developments in chitosan-based nanocomposites. In: Bio-based Polymers and Nanocomposites: Preparation, Processing, Properties & Performance, pp. 183–215. https://doi.org/10.1007/978-3-030-05825-8_9
14. Leceta, I., Guerrero, P., De La Caba, K.: Functional properties of chitosan-based films. Carbohydr. Polym. 93(1), 339–346 (2013). https://doi.org/10.1016/j.carbpol.2012.04.031
15. Bhatt, A.S., Bhat, D.K., Santosh, M.S.: Electrical and magnetic properties of chitosan-magnetite nanocomposites. Physica B. 405(8), 2078–2082 (2010). https://doi.org/10.1016/j.physb.2010.01.106
16. Wang, M.S., Wang, J.Y., Chen, Q., Peng, L.M.: Fabrication and electrical and mechanical properties of carbon nanotube interconnections. Adv. Funct. Mater. 15(11), 1825–1831 (2005). https://doi.org/10.1002/adfm.200500215
17. Gantayat, S., Rout, D., Swain, S.K.: Mechanical properties of functionalized multiwalled carbon nanotube/epoxy nanocomposites. Mater. Today Proc. 4(2), 4061–4064 (2017). https://doi.org/10.1016/j.matpr.2017.02.308
18. Manjappa, P., Rajan, H.K., Mahesh, M.G., Sadananda, K.G., Channegowda, M., Shivashankar, G.K., Mutt, N.B.: Effective attenuation of electromagnetic waves by synergetic effect of α-Fe2O3 and MWCNT/graphene in LDPE-based composites for EMI applications. Materials 15(24), 9006 (2022). https://doi.org/10.3390/ma15249006
19. Raja, M.M., Awal, R., Khandaker, J.I., Al-Mamun, M., Haque, M.M., Tanisa, N.Y., Farid, M.S., Hasan, S.M.S., Meherin, S.: HAP/f-MWCNTs/cobalt ferrites nano composites synthesis and electrical and magnetic performance investigation. Open Access Library J. 10(3), 1–15 (2023). https://doi.org/10.4236/oalib.1109875
20. Mergen, Ö.B., Arda, E., Evingür, G.A.: Electrical, optical and mechanical properties of chitosan biocomposites. J. Compos. Mater. 54(11), 1497–1510 (2020). https://doi.org/10.1177/0021998319883916
21. Ganji, P., Nazari, S., Zinatizadeh, A.A., Zinadini, S.: Chitosan-wrapped multi-walled carbon nanotubes (CS/MWCNT) as nanofillers incorporated into nanofiltration (NF) membranes aiming at remarkable water purification. J. Water Process Eng. 48, 102922 (2022). https://doi.org/10.1016/j.jwpe.2022.102922
22. Said, Z., Sohail, M.A., Walvekar, R., Liu, C.: Impact of sonication durations on thermophysical properties, contact angle and surface tension of f-MWCNTs nanofluid for heat transfer. J. Mol. Liq. 358, 119164 (2022). https://doi.org/10.1016/j.molliq.2022.119164
23. Rafique, I., Kausar, A., Anwar, Z., Muhammad, B.: Exploration of epoxy resins, hardening systems, and epoxy/carbon nanotube composite designed for high performance materials: A review. Polym. Plast.

Technol. Eng. 55(3), 312–333 (2016). https://doi.org/10.1080/03602559.2015.1070874
24. Akhter, S., Basirun, W.J., Alias, Y., Johan, M.R., Bagheri, S., Shalauddin, M., Ladan, M., Anuar, N.S.: Enhanced amperometric detection of paracetamol by immobilized cobalt ion on functionalized MWCNTs-Chitosan thin film. Anal. Biochem. 551, 29–36 (2018). https://doi.org/10.1016/j.ab.2018.05.004
25. Yahya, N., Koziol, K., Boskovic, B.O., Yahya, N.: Synthesis of carbon nanostructures by CVD method. In: Carbon and Oxide Nanostructures: Synthesis, Characterisation and Applications, pp. 23–49 (2011). https://doi.org/10.1007/8611_2010_12
26. Oyetade, O.A., Nyamori, V.O., Martincigh, B.S., Jonnalagadda, S.B.: Effectiveness of carbon nanotube–cobalt ferrite nanocomposites for the adsorption of rhodamine B from aqueous solutions. RSC Adv. 5(29), 22724–22739 (2015). https://doi.org/10.1039/C4RA15446K
27. Santangelo, S., Piperopoulos, E., Fazio, E., Faggio, G., Ansari, S., Lanza, M., Neri, F., Milone, C.: A safer and flexible method for the oxygen functionalization of carbon nanotubes by nitric acid vapors. Appl. Surf. Sci. 303, 446–455 (2014). https://doi.org/10.1016/j.apsusc.2014.03.023
28. Hamilton Jr, R.F., Xiang, C., Li, M., Ka, I., Yang, F., Ma, D., Porter, D.W., Wu, N., Holian, A.: Purification and sidewall functionalization of multiwalled carbon nanotubes and resulting bioactivity in two macrophage models. Inhalation Toxicol. 25(4), 199–210 (2013). https://doi.org/10.3109/08958378.2013.775197
29. Rasweefali, M.K., Sabu, S., Azad, K.M., Rahman, M.R., Sunooj, K.V., Sasidharan, A., Anoop, K.K.: Influence of deproteinization and demineralization process sequences on the physicochemical and structural characteristics of chitin isolated from Deep-sea mud shrimp (*Solenocera hextii*). Adv. Biomarker Sci. Technol. 4, 12–27 (2022). https://doi.org/10.1016/j.abst.2022.03.001
30. El Knidri, H., Belaabed, R., Addaou, A., Laajeb, A., Lahsini, A.: Extraction, chemical modification and characterization of chitin and chitosan. Int. J. Biol. Macromol. 120, 1181–1189 (2018). https://doi.org/10.1016/j.ijbiomac.2018.08.139
31. Teli, M.D., Sheikh, J.: Extraction of chitosan from shrimp shells waste and application in antibacterial finishing of bamboo rayon. Int. J. Biol. Macromol. 50(5), 1195–1200 (2012). https://doi.org/10.1016/j.ijbiomac.2012.04.003
32. Boudouaia, N., Bengharez, Z., Jellali, S.: Preparation and characterization of chitosan extracted from shrimp shells waste and chitosan film: Application for Eriochrome black T removal from aqueous solutions. Appl. Water Sci. 9(4), 91 (2019). https://doi.org/10.1007/s13201-019-0967-z
33. Zaman, A., Rashid, T.U., Khan, M.A., Rahman, M.M.: Preparation and characterization of multiwall carbon nanotube (MWCNT) reinforced chitosan nanocomposites: Effect of gamma radiation. BioNanoScience 5, 31–38 (2015). https://doi.org/10.1007/s12668-014-0159-0
34. Montoro, L.A., Rosolen, J.M.: A multi-step treatment to effective purification of single-walled carbon nanotubes. Carbon 44(15), 3293–3301 (2006). https://doi.org/10.1016/j.carbon.2006.06.018
35. Wang, S.F., Shen, L., Zhang, W.D., Tong, Y.J.: Preparation and mechanical properties of chitosan/carbon nanotubes composites. Biomacromolecules 6(6), 3067–3072 (2005). https://doi.org/10.1021/bm050378v
36. Al Sagheer, F.A., Al-Sughayer, M.A., Muslim, S., Elsabee, M.Z.: Extraction and characterization of chitin and chitosan from marine sources in Arabian Gulf. Carbohydr. Polym. 77(2), 410–419 (2009). https://doi.org/10.1016/j.carbpol.2009.01.032
37. Baharudin, L., Yip, A.C., Golovko, V.B., Polson, M.I., Aguey-Zinsou, K.F., Watson, M.J.: CO oxidation and the inhibition effects of carboxyl-modification and copper clusters on multi-walled carbon nanotubes. Appl. Catal. B. 262, 118265 (2020). https://doi.org/10.1016/j.apcatb.2019.118265
38. do Amaral Montanheiro, T.L., Cristóvan, F.H., Machado, J.P.B., Tada, D.B., Durán, N., Lemes, A.P.: Effect of MWCNT functionalization on thermal and electrical properties of PHBV/MWCNT nanocomposites. J. Mater. Res. 30(1), 55–65 (2015). https://doi.org/10.1557/jmr.2014.303
39. Thou, C.Z., Khan, F.S.A., Mubarak, N.M., Ahmad, A., Khalid, M., Jagadish, P., Walvekar, R., Abdullah, E.C., Khan, S., Khan, M., Hussain, S., Ahmad, I., Algarni, T.S.: Surface charge on chitosan/cellulose nanowhiskers composite via functionalized and untreated carbon nanotube. Arabian J. Chem. 14(3), 103022 (2021). https://doi.org/10.1016/j.arabjc.2021.103022
40. Osler, K., Twala, N., Oluwasina, O.O., Daramola, M.O.: Synthesis and performance evaluation of chitosan/carbon nanotube (chitosan/MWCNT) composite adsorbent for post-combustion carbon dioxide capture. Energy Procedia 114, 2330–2335 (2017). https://doi.org/10.1016/j.egypro.2017.03.1368
41. Jorio, A., Ferreira, E.H.M., Moutinho, M.V., Stavale, F., Achete, C.A., Capaz, R.B.: Measuring disorder in graphene with the G and D bands. Physica Status Solidi 247(11–12), 2980–2982 (2010). https://doi.org/10.1002/pssb.201000247
42. Cuentas-Gallegos, A.K., Frausto, C., Ortiz-Frade, L.A., Orozco, G.: Raman spectra of hybrid materials based on carbon nanotubes and Cs3PMo12O40. Vib. Spectrosc. 57(1), 49–54 (2011). https://doi.org/10.1016/j.vibspec.2011.05.003
43. He, X., Li, K., Xing, R., Liu, S., Hu, L., Li, P.: The production of fully deacetylated chitosan by compression method. Egypt. J. Aquat. Res. 42(1), 75–81 (2016). https://doi.org/10.1016/j.ejar.2015.09.003
44. Al Mgheer, T., Abdulrazzak, F.H.: Oxidation of multi-walled carbon nanotubes in acidic and basic Piranha mixture. Front. Nanosci. Nanotechnol. 2, 155–158 (2016). https://doi.org/10.15761/FNN.1000127
45. Hossain, M.A.F., Al-Mamun, M., Rahman, M.R., Hoque, S.M.: Effect of in-situ growth and separate addition method in hydrothermal process on the structural and magnetic properties of CoNiFe 2 O 4@ functionalized CNTs nanocomposite. Appl. Phys. A. 127, 1–21 (2021). https://doi.org/10.1007/s00339-021-05049-9
46. Hu, W.C., Sari, S.K., Hou, S.S., Lin, T.H.: Effects of acoustic modulation and mixed fuel on flame synthesis of carbon nanomaterials in an atmospheric environment. Materials 9(11), 939 (2016). https://doi.org/10.3390/ma9110939
47. Vejpravova, J., Pacakova, B., Kalbac, M.: Magnetic impurities in single-walled carbon nanotubes and graphene: A review. Analyst 141(9), 2639–2656 (2016). https://doi.org/10.1039/C6AN00248J
48. Xie, Y., Zhao, J., Le, Z., Li, M., Chen, J., Gao, Y., Y., Huang, Qin, Y., Zhong, R., Zhou, D., Ling, Y.: Preparation and electromagnetic properties of chitosan-decorated ferrite-filled multi-walled carbon nanotubes/polythiophene composites. Compos. Sci. Technol. 99, 141–146 (2014). https://doi.org/10.1016/j.compscitech.2014.05.013
49. Hu, C., Shen, F., Zhu, D., Zhang, H., Xue, J., Han, X.: Characteristics of Ti3C2X–chitosan films with enhanced mechanical properties. Front. Energy Res. 4, 41 (2017). https://doi.org/10.3389/fenrg.2016.00041
50. Backes, E.H., Sene, T.S., Passador, F.R., Pessan, L.A.: Electrical, thermal and mechanical properties of epoxy/CNT/calcium carbonate nanocomposites. Mater. Res. 21, e20170801 (2017). https://doi.org/10.1590/1980-5373-MR-2017-0801
51. Kodolova-Chukhontseva, V.V., Shishov, M.A., Kolbe, K.A., Smirnova, N.V., Dobrovol'skaya, I.P., Dresvyanina, E.N., Bystrov, S.G., Terebova, N.S., Kamalov, A.M., Bursian, A.E., Ivan'kova, E.M., Yudin, V.E.: Conducting composite material based on chitosan and single-wall carbon nanotubes for cellular technologies. Polymers 14(16), 3287 (2022). https://doi.org/10.3390/polym14163287
52. Martins, A.M., Eng, G., Caridade, S.G., Mano, J.F., Reis, R.L., Vunjak-Novakovic, G.: Electrically conductive chitosan/carbon scaffolds for cardiac tissue engineering. Biomacromolecules 15(2), 635–643 (2014). https://doi.org/10.1021/bm401679q

How to cite this article: Awal, R., Al-Mamun, M., Jewena, N., Khandaker, J.I., Tanisa, N.Y., Ahmed, S., Shahriar, F., Haque, M.M.: Upcycling prawn shells: Chitosan–carbon nanotube nanocomposites with boosted magnetic and electrical properties. Micro Nano Lett. 19, e12197 (2024). https://doi.org/10.1049/mna2.12197